



CrossMark  
click for updates

Cite this: *RSC Adv.*, 2016, 6, 10192

# Electrocoagulation by solar energy feed for textile wastewater treatment including mechanism and hydrogen production using a novel reactor design with a rotating anode

Ahmed Samir Naje,<sup>a</sup> Shreeshivadasan Chelliapan,<sup>\*a</sup> Zuriati Zakaria,<sup>b</sup> Mohammed A. Ajeel,<sup>c</sup> Kamaruzzaman Sopian<sup>d</sup> and Husam Abdulrasool Hasan<sup>d</sup>

This paper describes the treatment of textile wastewater using a unique design of an electrocoagulation (EC) reactor with a rotating anode. The effects of various operational parameters such as rotational speed of the anode, current density (CD), recirculation flow rate, operational time (RT) and continuous flow regime on the efficiency of pollutant removal in terms of chemical oxygen demand (COD) and colour were examined. The mechanisms of EC treatment and hydrogen production were also evaluated. In addition, the model verification was an attempt to study the passivation and adsorption phenomena. The results indicated that the optimum conditions were achieved at CD = 4 mA cm<sup>-2</sup>, RT = 10 minutes and rotational speed = 150 rpm, where the operating cost was 0.072 US\$ per m<sup>3</sup>. The removal efficiencies of COD and colour were 91%, 95% for the batch system and 91.5%, 95.5% for the continuous flow system respectively. Zeta potential values indicate that the chemical interaction happened, and XRD analysis of the sludge produced reveals that the reaction is a chemo-adsorption type, where the final product is environmentally friendly (aliphatic sludge). Hydrogen production was enhanced under the optimal conditions to produce 12.45%, reducing the power consumption by 9.4%. The passivation and adsorption resistance values validate the removal rate of pollutants.

Received 7th December 2015  
Accepted 11th January 2016

DOI: 10.1039/c5ra26032a

www.rsc.org/advances

## 1. Introduction

One of the most polluted types of wastewater is textile wastewater because of the big diversity of chemical additives and dyes contained in it, which make the additional treatment of the wastewater complicated. Recently, electrocoagulation (EC), as an efficient and eco-friendly process, has attracted considerable research attention. EC has been successfully used for the removal of pollutants from different industrial wastewaters such as laundry wastewater,<sup>1</sup> electroplating wastewater,<sup>2,3</sup> oil refinery wastewater,<sup>4</sup> restaurant wastewater,<sup>5</sup> metal plating wastewater<sup>6,7</sup> and poultry slaughterhouse wastewater.<sup>8,9</sup>

In this technique, the anode dissolves the coagulant (iron or aluminium electrodes) with an immediate production of hydrogen gas and hydroxyl ions at the cathode. The reactions at the anode, in the EC process including the electrodes of aluminium, are as follows.

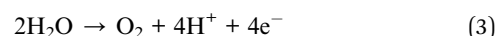
Anode:



The reaction at the cathode is:



When the anode potential is sufficiently high, the following secondary reaction can also happen at the anode:



The generated metallic ions go through further spontaneous reactions to give corresponding hydroxides which are insoluble. These hydroxides-metallic compounds have a strong affinity to adsorb the pollutants and eliminate them from the solution either by complexation or by electrostatic attraction, that is followed by coagulation.<sup>10-13</sup> Among the most critical tasks in decreasing the overall cost of the EC, the operation is the

<sup>a</sup>Department of Engineering, UTM Razak School of Engineering and Advanced Technology, Universiti Teknologi Malaysia, Jalan Semarak, 54100, Kuala Lumpur, Malaysia. E-mail: shreeshivadasan.kl@utm.my; Fax: +603-21805188; Tel: +603-21805178

<sup>b</sup>Department of Environmental Engineering and Green Technology, Malaysia-Japan International Institute of Technology (MIIT), Universiti Teknologi Malaysia, Jalan Semarak, 54100, Kuala Lumpur, Malaysia

<sup>c</sup>Department of Chemical Engineering, Faculty of Engineering, University of Malaya, 50603 Kuala Lumpur, Malaysia

<sup>d</sup>Solar Energy Research Institute, Universiti Kebangsaan Malaysia, 43600, Bangi, Selangor, Malaysia

reduction of the internal resistance drop of the electrodes (*IR*-drop) to improve the performance of the current. Both hydrogen and oxygen gas are evolved near the anode and cathode as each gas bubble nucleates. These bubbles are in the form of insulating spherical figures (passivation film), and if permitted to gather on the surfaces of the electrode, will increase the cell's overall electrical resistance, thus requiring a greater amount of electrical energy to obtain the optimum removal efficiency.<sup>12,14</sup>

In the existing literature, the EC process has been performed using various model designs, such as parallel electrodes configurations,<sup>6,15,16</sup> twenty-five pairs circular shape of electrode,<sup>10</sup> a packed bed cylindrical electrode,<sup>17</sup> a fixed bed reaching electrode,<sup>18</sup> and a hollow cylindrical electrode.<sup>19</sup> These electrode designs have commonly considered the same approach and are not focused on reducing these fouling films from the surface of the electrode without adding any chemicals. However, in the operation, an oxide fouling film created on the surface of static electrodes with no liquid mixing can produce poor diffusion and transfer of mass, and this decreases the operation's overall performance levels and increases the overall consumption of energy.<sup>20</sup> To mitigate the accumulation of bubbles, the flow of the electrolyte surrounding the electrodes must be increased to push the bubbles out.<sup>14</sup> This may be achieved by improving the state of turbulence, and at the same time, the mass transport may be improved by increasing the turbulence state within the flow *via* an EC reactor. Alternatively, the turbulence may be increased by raising the flow rate rather than the EC reactor. The increase in the turbulence state also reduces the passivation at the electrode plates. The overall intensity of the turbulence is the main reason for the micro-mixing operations (eddy diffusion of the momentum), heat values and mass values.<sup>21</sup> Consequently, micro-mixing operations limit the overall development of rapid reactions.

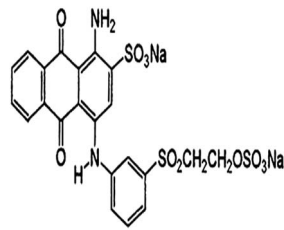
To address these effects, in this study, a unique design of an EC reactor that includes a rotating impellers anode was analyzed and practical investigations were conducted to improve the overall efficiency of this type of reactor. The main goal of this research is to evaluate the influences of operational parameters, such as the rotational speed of the anode, current density, EC reaction time. Moreover, to investigate the effect of recirculation flow rate of the wastewater and continuous flow system on the removal efficiency of textile wastewater pollutants. The mechanism of EC treatment and hydrogen production were also investigated. To our knowledge, the enhancement of hydrogen production from the EC process has not been reported earlier. In addition, the unique design is verified by studying the effect of the rotational speed on the reactivity of the anode (passivation and adsorption phenomenon).

## 2. Materials and methods

### 2.1. Wastewater characteristics

In this work, the wastewater was collected from a textile producer in Malaysia – Kuala Lumpur (Kajang). The company uses reactive blue 19 (Remazol brilliant blue R dye) for the fabric dyeing process. Table 1 presents the main characteristics of the textile wastewater and the properties of the Remazol brilliant blue R, respectively.

**Table 1** Characteristics of textile wastewater and properties of reactive blue 19 dye

Parameters	Values and colour properties
Electrical conductivity ( $\mu\text{S cm}^{-1}$ )	19 000
COD ( $\text{mg L}^{-1}$ )	4010
pH	7.00
Colour generic name	Reactive blue 19
Synonym	Remazol brilliant blue R
Chemical structure	
Chemical formula	$\text{C}_{22}\text{H}_{16}\text{O}_{11}\text{N}_2\text{S}_3\text{Na}_2$
Molecular weight ( $\text{g mol}^{-1}$ )	626.50
$\lambda_{\text{max}}$ <sup>a</sup> (nm)	455
<sup>a</sup> Absorbance of 1530 PtCo at 455.	

### 2.2. Description of EC rotating anode reactor

The novel EC closed reactor that is used in this investigation and its schematic representation are illustrated in Fig. 1a. The reactor with 10 L working volume had a stirred tank setting of the cylindrical form (external diameter, 180 mm; inner diameter, 174 mm; total length, 500 mm) and was constructed from perspex. A rotating shaft (diameter, 32 mm) was attached to a motor with adjustable speed in order to hold the impeller structure and also to maintain the electrode rotations. The motor is DC electrical type and supplies various steady state speeds (0–1000 rpm, USA). The electrodes were made of aluminium (Al). The rotating anode was composed of 10 impellers with 10 rings used as the cathode. As shown in Fig. 1b, each impeller was composed of four main rods (length, 30 mm; diameter, 12 mm) and the rings (diameter, 172 mm; internal diameter, 134 mm; thickness, 12 mm) were arranged 30 mm apart from each other. The total active surface area of the reactor was 500 cm<sup>2</sup>. The reactor contained three equally spaced baffles to stop the rotation and the tangential flow arrangement of the mass fluid, as well as to establish the cathode rings.

### 2.3. Experimental procedure

The EC reactor's performance was characterised in terms of chemical oxygen demand (COD) and colour removal. The experiment was carried out initially in a batch system by studying the effect of the rotational speed of the anode and current density. The overall efficiency of the reactor was tested using three main variables; processing time, current density and the anode's overall rotational speed. The electrolysis time (RT) was maintained in the range of 10 to 30 minutes. Six main current densities (CD); 2, 4, 6, 8, 10, 12 mA cm<sup>-2</sup> with various steady-state anode rotational speeds of 0, 75, 100, 150, 200 and 250 rpm were examined. In every execution, a 10 L sample was

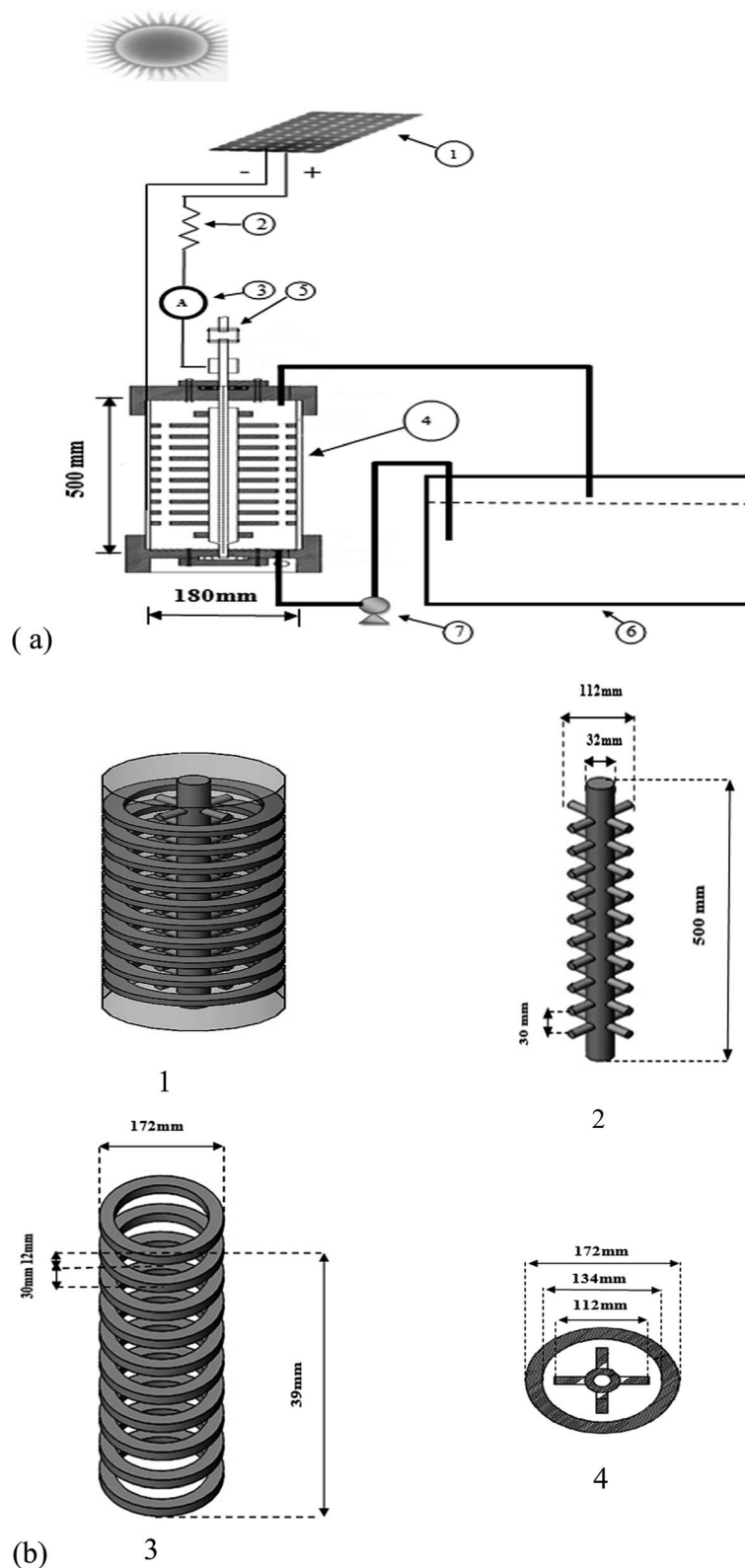


Fig. 1 (a) Schematic diagram of EC experimental setup: (1) solar energy supply; (2) variable resistance; (3) ammeter; (4) EC reactor; (5) motor variable speed; (6) reservoir; (7) peristaltic pump; (b) configurations of electrodes: (1) anode and cathode; (2) impellers of anode; (3) rings of cathode; (4) top view of impellers anode and rings cathode.

utilized for the operation of EC treatment at room temperature (25 °C). The EC batch rounds were executed 72 times, for real textile wastewater were 36 times and for synthetic reactive blue 19 dye were 36 times. The colour experiment investigations (removal rate and sludge characterization studies) were performed for the 300 mg L<sup>-1</sup> of reactive blue 19 dye. A primary sample was extracted and subsequently, at the end of each round, the cells were cleaned with a 5% hydrochloric acid solution for 10 minutes and later scrubbed with a sponge.

Both the cathode and anode were attached to the negative and positive parts of a solar energy cell (TPSM6U-300 W, maximum current 8.02 A, maximum voltage 37.42 V, dimensions 1956 × 992 mm, 72 cells). The solar panel was fed by the sun simulator artificial light inside the lab to ensure continuity of energy. The sun simulator consists of 45 halogen lamps, each with rated power of 300 W. The lamps is arranged in 10 rows on 1.7 m × 3.6 m with each row consists of 5 or 4 lamps with center-to-center distance is about 40 cm. Each lamp is equipped with a dimmer in order to set the lamp's radiation. The source of electricity is supplied from public electricity line, which is installed in the laboratory. The simulator may produce varieties of radiation values with small errors. The average radiation is 400 watt m<sup>-2</sup> to 1100 watt m<sup>-2</sup> with errors about of 3.16% to 4.05%. The main voltages were around 15–18.5 V. The current and voltage were maintained as invariant in every round with the use of a variable resistance and estimated using an ammeter (Heme Analyst 2050, EU). In every iteration, the samples were allowed to settle for 30 minutes and then filtered. Approximately 50 mL of supernatant sample was gathered for analysis and investigation in replicate. Similar parameters were estimated in every replicate sample.

The entire experiment was carried out six times to obtain advanced investigations for the recirculation flow rate effect, continuous flow system, mechanism of treatment including zeta potential and sludge study, hydrogen production and reactivity of the electrode.

**2.3.1. Recirculation flow rate effect and continuous flow system.** For the study of the influence of the recirculation flow rate, textile wastewater was fed at the bottom of the reactor by a peristaltic pump (Masterflex B/T series). The system was run while electrolysis in semi-continuous mode and 20 L of textile wastewater was kept in a tank and continuously recycled to the reactor. The effectiveness of the EC process in a nonstop flow system was examined at optimal operation conditions of the batch EC system.

**2.3.2. Mechanism of treatment.** The stability of a pollutant during the EC process is determined using a zeta potential test for particles' electrical charge. For the sludge characterization study, the EC was operated for a certain time, and then the sludge produced through the EC process was filtered. The precipitate was then dried in an oven before being ground into a fine powder. Furthermore, to examine the nature of the sludge produced during EC, this powder was characterized by XRD analysis.

**2.3.3. Hydrogen production.** For estimation of hydrogen production, a hydrogen gas detector (TS-4000EX Series, flow rate 0–1000 mL min<sup>-1</sup>, 4–20 mA DC output signal) was

connected directly with the EC reactor to record the values of H<sub>2</sub> by volume as percent from the total volume of gas inside the reactor (5 cm height, 1.189 L volume). Hydrogen production was conducted using real textile wastewater on the rotational speed of the anode and the EC reaction time.

**2.3.4. Passivation and adsorption phenomenon by impedance.** The electrochemical impedance spectroscopy experiments were performed with the potential amplitude of the AC signal kept at 10 mV, and the measured frequency range was 0.01–10<sup>5</sup> Hz. An EC-Lab SP-300 potentiostat with EC-Lab software V10.12 was used to perform the electrochemical impedance assays. Impedance runs were carried out in a single-compartment, three-electrode system, which consisted of an aluminium electrode (1 : 25 of the original size) as the working electrode, Ag/AgCl (3 M KCl) electrode as a reference electrode, and a platinum wire as counter electrode.

## 2.4. Chemical analysis

The overall treatment performance of the novel electrolysis was analyzed regarding COD and colour removal performances. The COD was measured by the dichromate method. The suitable sample for measurement of COD was introduced into a prepared solution of (0–1500 mg L<sup>-1</sup>) including mercuric sulfate, H<sub>2</sub>SO<sub>4</sub> and potassium dichromate and the mixture was then brooded for 2 h at 150 °C in an HACH/DRB 200 thermo-reactor for COD and thermal digestions. COD concentration was measured colorimetrically using an HACH DR 2800 spectrophotometer. The colour was also estimated using a Hach DR 2800 spectrophotometer. The pH was measured by PHM84 meter and the conductivity with an EC400 ExStik from Extech Instruments. The samples were filtered using a Fiononi 603 filter paper with pore size 0.45 μm. The rotational speed of the rotated anode was maintained by a microprocessor digital meter. To define the zeta potential of flocs formed by electrolysis, a zeta potential analyzer (Zetasizer Nano-ZS, Malvern Instruments) was used. XRD analysis was carried out to examine the EC sludge's crystalline phase. The powder XRD patterns were recorded using an X-ray diffractometer (Bruker/D8 Advance). All the analytical work was conducted according to the procedures prescribed in the standard methods.<sup>22</sup> The computation of COD and colour removal was carried out using formulas specified in other works.<sup>13,17</sup>

## 2.5. Analysis of current performance, electrode and power consumption and operational cost

The current performance is a critical parameter that affects the overall electrode lifetime in electrocoagulation operations. Abdel-Gawad *et al.* (2012) reported that the efficiency of the current is the ratio of the amount of Al used ( $\Delta M_{\text{exp}}$ ) to the overall theoretical value ( $\Delta M_{\text{theo}}$ ).<sup>23</sup>

$$\text{CE} = \Delta M_{\text{exp}} / \Delta M_{\text{theo}} \times 100 \quad (4)$$

The level of theoretical Al dissolution is computed based on Faraday's law:<sup>23</sup>

$$Al_{\text{theoretical}}^{3+} = M \times I \times RT/ZFV \quad (5)$$

where  $M$  = molecular mass of Al (26.98 g mol<sup>-1</sup>),  $I$  = electrical current (A),  $RT$  = reaction time of EC (s),  $Z$  = amount of electron moles (3),  $F$  = Faraday's constant (96 500 C mol<sup>-1</sup>), and  $V$  = volume of wastewater (L). A weighing process determined the Al amount used on the electrodes prior and after every iteration, and the weight loss for the Al was computed.

The operation cost in the wastewater treatment consists of the electricity costs, sludge disposal cost, the chemical reagents, maintenance, labour, and equipment. During the electrochemical operation, the most significant parameters that affect the operating cost are the cost of the electrical energy consumed and the electrode material. Therefore, these factors are computed during the investigation to identify the overall operating costs:<sup>11</sup>

$$\text{Operating cost} = aC_{\text{energy}} + bC_{\text{electrode}} \quad (6)$$

$$C_{\text{energy}} = U \times I \times RT/V \quad (7)$$

where  $C_{\text{energy}}$ ,  $C_{\text{electrode}}$ ,  $a$ ,  $b$ , and  $U$  represent energy consumption for each cubic meter of wastewater (kW h m<sup>-3</sup>), electrode consumed for treatment of one cubic meter of wastewater (kg m<sup>-3</sup>), electricity cost 0.080 US\$ per kW h and standard cost of aluminium 2.5 US\$ per kg, voltage (V), respectively.

In this study, the overall electrical energy consumption was computed based on the following equation:

$$C_{\text{energy}} \text{ (kW h m}^{-3}\text{)} = (C_{\text{energy}})_{\text{S}} + (C_{\text{energy}})_{\text{M}} \quad (8)$$

where  $(C_{\text{energy}})_{\text{S}}$  represents the value of the electrical energy consumption of the reactor (electricity input to the anode and the cathode due to DC solar cell), and  $(C_{\text{energy}})_{\text{M}}$  represents the electrical energy consumption rate of the DC motor anode rotation. Both  $(C_{\text{energy}})_{\text{S}}$  and  $(C_{\text{energy}})_{\text{M}}$  were computed from eqn (7). The operating expense is computed based on the prices acquired from the Malaysia market in the year 2015.

## 2.6. Analysis of the theoretical hydrogen yield

According to the stoichiometry of the reduction and oxidation reactions at cathodes and anodes, when 1 mole of Al loses 3 moles of electrons by oxidation of the anodes, water electrolysis at the cathodes produces 1.5 moles of hydrogen. Likewise, for iron anodes, when 1 mole of Fe loses 2 moles of electrons at the anodes, 1 mole of hydrogen is formed at the cathodes.

In the EC process, the reduction and oxidation reactions are initiated by providing the electrodes with direct current. Eqn (9) gives the relation between the amount of hydrogen generated and the supplied current:<sup>10</sup>

$$n_{\text{H}_2} = (I \times RT/F) \times H \quad (9)$$

Likewise, the relationship between the amount of hydrogen generated, the effective electrode area and the supplied current density is as shown in eqn (10):

$$n_{\text{H}_2} = (J \times A \times RT/F) \times H \quad (10)$$

where  $n_{\text{H}_2}$  is the amount of hydrogen generated (mol),  $I$  is the supplied current (A),  $J$  is the supplied current density (CD, mA m<sup>-2</sup>),  $A$  is the area of the effective electrode (m<sup>2</sup>),  $H$  is the number of hydrogen molecules generated per electron included in the redox reactions. The value of  $H$  is independent of the type of anode, aluminium or iron, and in both cases is equal to 1/2.

The amount of hydrogen gas produced by volume can be calculated using the following equation:<sup>24</sup>

$$P \times V_{\text{H}_2} = (m_{\text{H}_2}/M_{\text{H}_2}) \times R \times T \quad (11)$$

where  $P$  denotes pressure in atm;  $V_{\text{H}_2}$  denotes the volume of the cumulative hydrogen (L);  $m_{\text{H}_2}$  denotes the mass of the produced cumulative hydrogen in a certain time (g);  $M_{\text{H}_2}$  is the hydrogen's molar mass (2 g mol<sup>-1</sup>),  $T$  is room temperature (25 °C), and  $R$  is the gas constant (0.082 L atm mol<sup>-1</sup> K<sup>-1</sup>).

The energy contents of the hydrogen gas (kW h m<sup>-3</sup>) can be calculated from the following equation:<sup>24</sup>

$$E_{\text{H}_2} \text{ (kW h m}^{-3}\text{)} = \frac{m_{\text{H}_2} \times 122}{V \times 3600} \quad (12)$$

where  $E_{\text{H}_2}$  is calculated based on the hydrogen energy yield of 122 kJ g<sup>-1</sup> and 1 kW h = 3600 kJ.

## 3. Results and discussion

### 3.1. EC treatment of textile wastewater and reactive blue 19

In EC batch system, the effect of rotational speed of anode, current density and reaction time have been studied to investigate the optimal operational conditions. The effect of recirculation flow rate and EC continuous flow system on pollutants removal efficiency were also investigated according to the optimal conditions result of EC batch system.

#### 3.1.1. Effect of operational conditions of EC batch system.

The rotational speed is an important parameter to move the coagulant substance that is formed and affects the electrodes dissolution rate in the reactor. This parameter is responsible for the homogeneity of the reactor's contents. The rotational speed may also lead to the homogenization of the reactor variables, including the temperature and pH.<sup>8</sup> On the other hand, a high rotational speed can potentially damage flocs that are formed within the reactor, and create smaller flocs that are not easy to extract from the water. In this study, the impact of rotational speed was analyzed at 0, 75, 100, 150, 200 and 250 rpm, with current densities (CD) of 2, 4, 6, 8, 10 and 12 mA cm<sup>-2</sup> and with the electrolysis time (RT) of 10 to 30 minutes.

In terms of a stirred tank, the Reynolds number is commonly utilized:<sup>20</sup>

$$Re = \rho ND^2/\mu \quad (13)$$

where  $\rho$  = density,  $\mu$  = viscosity,  $D$  = impeller bar length (at  $D$  = 11.20 cm), and  $N$  = impeller revolutions (per second). At standard room temperature (25 °C), the wastewater viscosity and density are  $\mu = 0.8937 \times 10^{-3}$  Pas and  $\rho = 997.04$  kg m<sup>-3</sup> respectively. When the rotational speed ( $N$ ) is 75, 100, 200, 150, and 250 rpm, the corresponding Reynolds number (Re) is

17 565, 23 420, 35 130, 46 840 and 58 550 respectively. This confirms that it is an entirely turbulent flow ( $Re > 10^4$ ).

Based on the experimental results depicted in Fig. 2a (I to VII), when the anode was static with no rotational speed ( $CD = 10 \text{ mA cm}^{-2}$ ), the corresponding COD removal efficiency was 63%, in a period of 30 minutes. The COD removal efficiency increased to 71% and 79% within 10 minutes (processing time reduced by 20 minutes) when the reactor was operated at a rotational speed of 75 and 100 rpm respectively and the current density reduced to  $CD = 4 \text{ mA cm}^{-2}$ . Further increases

in rotational speed (150 rpm) resulted in higher COD removal (91%) in the same operating conditions of reaction time (10 minutes) and current density ( $4 \text{ mA cm}^{-2}$ ). It is clear that the COD removal efficiency increased with increasing rotational speed of the anode, starting from 0 to reach its highest values at 150 rpm and then decreasing at 200 and 250 rpm for all current density and reaction time values. COD removal was 46%, 55%, 58%, 63%, 60% and 51% for 0, 75, 100, 150, 200, and 250 rpm respectively at current density  $CD = 2 \text{ mA cm}^{-2}$  and 10 min reaction time. During this period, the  $\text{Al}(\text{OH})_3$  flocs were

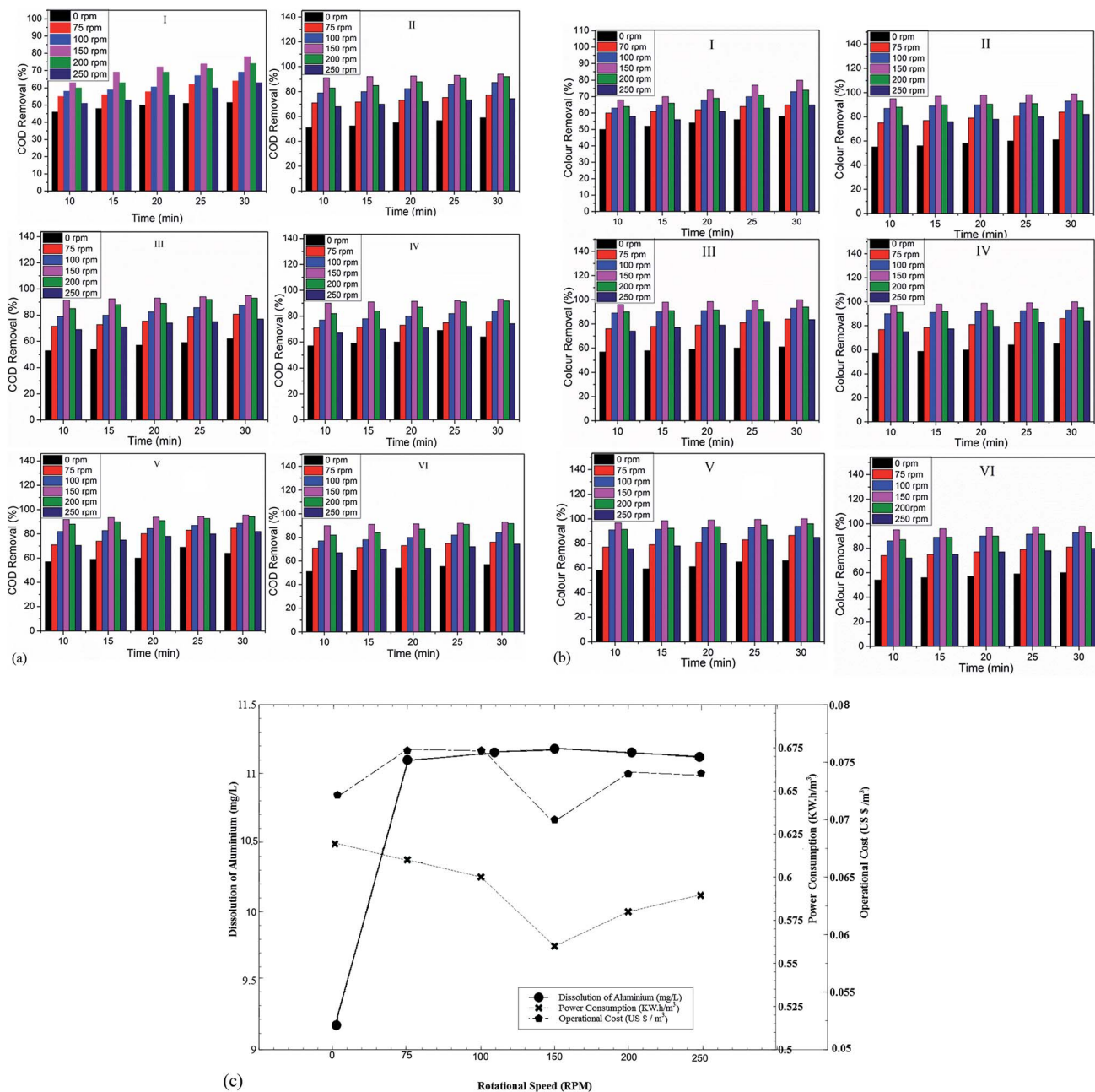


Fig. 2 (a) Effect of rotational speed on COD removal of real textile wastewater: (I)  $CD = 2 \text{ mA cm}^{-2}$ ; (II)  $CD = 4 \text{ mA cm}^{-2}$ ; (III)  $CD = 6 \text{ mA cm}^{-2}$ ; (IV)  $CD = 8 \text{ mA cm}^{-2}$ ; (V)  $CD = 10 \text{ mA cm}^{-2}$ ; (VI)  $CD = 12 \text{ mA cm}^{-2}$ ; (b) effect of rotational speed on colour removal (reactive blue 19): (I)  $CD = 2 \text{ mA cm}^{-2}$ ; (II)  $CD = 4 \text{ mA cm}^{-2}$ ; (III)  $CD = 6 \text{ mA cm}^{-2}$ ; (IV)  $CD = 8 \text{ mA cm}^{-2}$ ; (V)  $CD = 10 \text{ mA cm}^{-2}$ ; (VI)  $CD = 12 \text{ mA cm}^{-2}$ ; (c) effect of anode rotational speed on dissolution of aluminium, power consumption and operational cost at conditions ( $CD = 4 \text{ mA cm}^{-2}$ ,  $RT = 10 \text{ min}$ ).

connected to each other, and precipitation was easier. However, when the rotational speed was increased to 200, and 250 rpm, no increase of COD removal efficiency was observed, probably due to the extremely high rotational speed causing the flocs to become degraded by collisions with each other.<sup>8,12</sup> It should be mentioned here that the increase in the COD removal efficiency resulted from the increase in the overall current density.<sup>25</sup> There was a significant change in the COD removal when the current density increased to  $CD = 2$  to  $4 \text{ mA cm}^{-2}$ , with values of 52, 71, 79, 91, 83 and 69% for 0, 75, 100, 150, 200, and 250 rpm respectively at the first 10 min. After that, for the same reaction time (RT = 10 min), the COD removal efficiency increased from 52% to 54%, 71% to 72%, 79% to 82%, 91% to 93%, 83% to 88%, 69% to 70.5% for current densities of 4 and  $10 \text{ mA cm}^{-2}$  and rotational speeds of 0, 75, 100, 150, 200, and 250 rpm, respectively. At current density  $CD = 12 \text{ mA cm}^{-2}$  there was an adverse effect on the removal efficiency. A limited difference was observed in the removal efficiency when the current density increased. When the initial concentration of COD is high ( $4010 \text{ mg L}^{-1}$ ), there is no significant effect of the current density on the removal rate, especially at the first reaction time.<sup>26</sup>

The main results were in line with the remaining contaminated properties of colour at all the current density and rotational speed values (Fig. 2b (I–VII)). The colour was decreased from 1530 PtCo to 489, 76.50, 61.20, 53.55, 49.73 and 76.6 PtCo during the initial 10 minutes with a rotational speed of 150 at current densities of 2, 4, 6, 8, 10, and  $12 \text{ mA cm}^{-2}$  respectively. Thus, additional experiments were continued at  $4 \text{ mA cm}^{-2}$  so as to avoid additional consumption of energy.

Fig. 2c depicts the quantity of aluminium dissolved, power consumption, and operational cost with current density  $CD = 4 \text{ mA cm}^{-2}$  at conditions of 0, 75, 100, 150, 250 rpm, and 10 minutes. The dissolution of aluminium was increased with the increase in the rotational speed, where the quantity was  $9.15 \text{ mg L}^{-1}$  for the static case and increased to a maximum value of  $11.18 \text{ mg L}^{-1}$  at 150 rpm. This increase due to passivation of the anode reduced with increasing rotational speed as a result of creating turbulence.<sup>12,14</sup> This behaviour has an effect on the current efficiency (eqn (4)), where  $CE = 81\%$  in the static case and increased to a typical value of  $CE = 100\%$  at 150 rpm. Hence, the main voltage decrease with increasing rotational speed showed values of 18.5, 17, 16.30, 15.10, 15.00 and 15.00 V for 0, 75, 100, 150, 200, and 250 rpm respectively. The current and voltage consumption for the motor to rotate the anode were (0.8 A, 3.9 V), (0.9 A, 4 V), (1 A, 4 V), (1.2 A, 4.3 V), (1.4 A, 4.5 V) for 75, 100, 150, 200, and 250 rpm respectively. The minimum overall electrical energy consumption (eqn (7) and (8)) was  $0.56 \text{ kW h m}^{-3}$  at 150 rpm. As a result, there was no significant difference in the operational cost (eqn (6)) with respect to the rotational speed at the same current density ( $4 \text{ mA cm}^{-2}$ ) and the minimum cost was 0.072 US\$ per  $\text{m}^3$  at 150 rpm. Thus, EC treatment at  $4 \text{ mA cm}^{-2}$ , 150 rpm and 10 minutes reaction time is typically required.

**3.1.2. Effect of wastewater recirculation flows rate.** The selection of the flow system depends on the amount of wastewater to be treated. In this study 20 L of wastewater was constantly recirculated from reservoir to reactor in a continuous

flow throughout the EC. However, the influence of the recirculation flow rate was observed for flow rates of 6, 12 and  $21 \text{ L min}^{-1}$  at fixed parameters of operation:  $4 \text{ mA cm}^{-2}$  and 150 rpm. Fig. 3a displays the COD removal at various flow rates. The concentrations of COD for the assays of 6, 12 and  $21 \text{ L min}^{-1}$  at 10 min were 802, 1042.5 and  $1283 \text{ mg L}^{-1}$  respectively. At the higher flow rate, lower COD removal was detected, and this was associated with the hydraulic retention time in the reactor. The flow of aluminium ions in the electrochemical reactor is assumed to be fast, but more time was needed for the process of coagulation in the bulk and the flow of released ions from the anodic surface to the bulk. So higher removal efficiency is associated with a lower flow rate, which is related to a higher retention time. At 30 min of the EC treatment, the effectiveness of the COD removal achieved (93%, 92%, 91.6%) was approximately comparable to all the recirculation flow rates reported. Earlier reports<sup>17,27</sup> also mentioned this point, that the removal

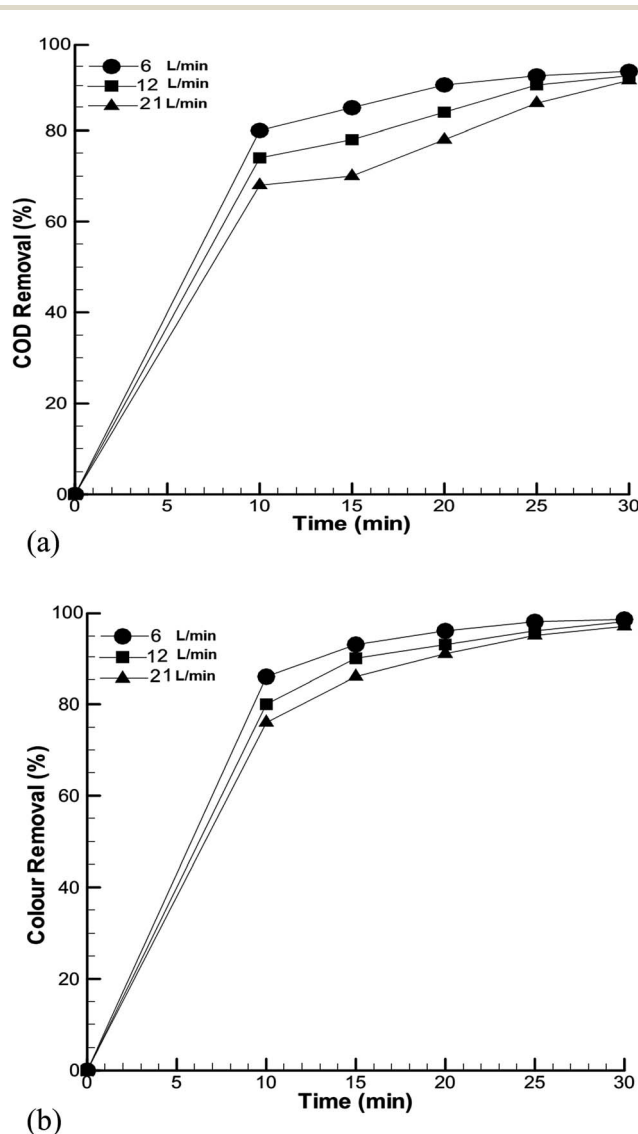


Fig. 3 Effect of recirculation flow rate at conditions ( $CD = 4 \text{ mA cm}^{-2}$ , 150 rpm) on: (a) COD removal (%); (b) colour removal (%).

effectiveness decreased with the increase of the inlet flow rate. Fig. 3b demonstrates the colour removal with flow rates of 6, 12, and 21 L min<sup>-1</sup>. After 15 min, a colour removal effectiveness of >91% was found for all the wastewater recirculation flow rates.

**3.1.3. EC process in continuous flow system.** In order to regulate the influence of the flow regime on the reactor performance, one experiment was carried out with a constant flow system. The system efficiency in a constant flow system was examined with operational parameters of  $Q = 0.333$  L min<sup>-1</sup> flow rate (related to a retention time of 30 min), 4 mA cm<sup>-2</sup> current density, rotational speed 150 rpm, and pH of 7. During the experiment, effluent samples were taken at different times, and the experiment continued until steady-state concentrations were achieved.

After 20 min of the EC process, the system reached a steady state and then the effluent COD concentration was approximately constant, as shown in Fig. 4. The concentration of the effluent COD decreased from 4010 to 341 mg L<sup>-1</sup> at 10 min (91.50% removal) to 200.50 mg L<sup>-1</sup> at 20 min (95% removal). With a single pass of wastewater with a 30 min retention time, 95.50% removal efficiency of COD was achieved. On the other hand, the reactive blue 19 color reading index has been reduced to 68.85 PtCo at 10 min, corresponding to a 95.50% removal efficiency.

### 3.2. Mechanism of treatment

The reaction mechanism of EC treatment has been studied using zeta potential and XRD techniques to elucidate the reaction behavior of aluminium hydroxyl with pollutants during the treatment process.

**3.2.1. Zeta potential determination.** The stability of a pollutant is defined by its physicochemical properties. Several pollutants are collections of particles of similar charge that repel each other, with the repulsive forces creating a colloidal, stable system. The (charged) pollutant particles attract oppositely charged ions to maintain their electroneutrality. The

attraction of counter-ions to a pollutant that is negatively charged gives an electric double layer divided into a Stern and diffuse layer. It is hard to determine the charge at the colloid surface because of the concentrations of the charge in the Stern and diffuse layers. Therefore, as the particle transfers over the solution, the zeta potential is used as an investigational measure of its effective charge, providing a direct indicator of the stability of the solution. The role of the aluminium matrix generated through electrolysis is to destabilize the colloidal suspension by reducing the attractive forces, thus lowering the energy barrier and enabling particles to be aggregated. The zeta potential decreases with increasing pH,<sup>28,29</sup> so the pH in the experiment is kept at the natural value of the wastewater (pH = 7).

Fig. 5 presents zeta potential measurements for the EC process as a function of electrolysis time along with a COD concentration in conditions of 4 mA cm<sup>-2</sup>, 150 rpm, and pH 7. At the beginning of the EC process (5 min electrolysis time), no very significant change is observed because the low ionic concentrations limit the possible coagulation mechanism. As a result, increasing the electrolysis time will increase the aluminium concentration in solution. The addition of aluminium coagulant could contain the electric double layer around the colloidal particles, decreasing repulsion and encouraging aggregation of the pollutant. Cationic coagulants provide positive electric charge to reduce the negative charge (zeta potential) of particles.<sup>30</sup> Since the amount of aluminium dissolved at the anode increases, the residual COD concentration is decreased and the zeta potential increases. As the system moved into more electrolysis time (>10 min), the rate of COD removal continued to decrease from 360 to 240 mg L<sup>-1</sup>, while the zeta potential increased from 29 to 33 mV. As noted in Section 3.1.1, the optimum reaction time was found to be 10 min for reducing the COD concentration from 4010 to 360 mg L<sup>-1</sup> at CD = 4 mA cm<sup>-2</sup> and 150 rpm. It seems that after 10 min reaction time, the low increase in zeta potential indicates stabilization of the solution when COD removal is slow in the

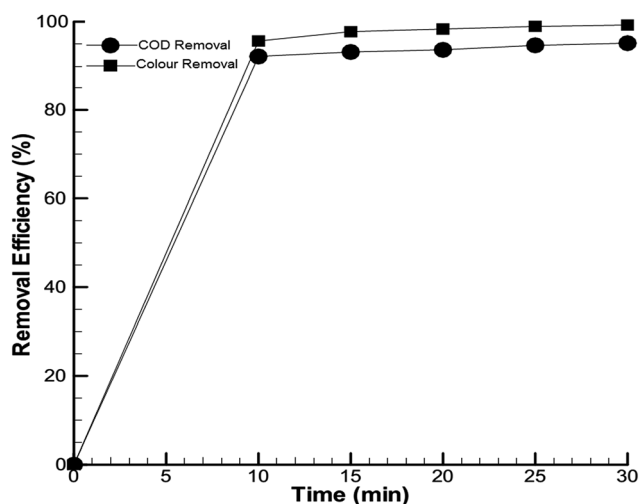


Fig. 4 EC process at a continuous flow system with conditions (CD = 4 mA cm<sup>-2</sup>, 150 rpm,  $Q = 0.333$  L min<sup>-1</sup> and pH of wastewater = 7).

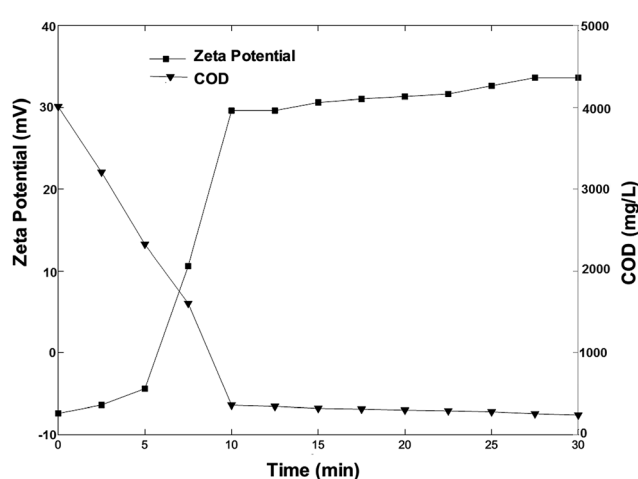


Fig. 5 Variation of zeta potential and residual COD concentration in solution with respect to electrolysis time at conditions (4 mA cm<sup>-2</sup>, 150 rpm and pH of wastewater = 7).



stable stage. The slow change of zeta potential reveals there was a dropping in the reaction rate between aluminium hydroxyl and the pollutants, where the decreasing of COD concentration leads to reduction in reaction rate.

**3.2.2. XRD characterization of sludge.** Commonly, the electrocoagulation mechanism for treatment of wastewater is complicated. The process of removal of COD may include electrochemical adsorption and oxidation by physical entrapment and electrostatic attraction. Yet, the colour removal may include, in addition to adsorption, complexation with the aluminium hydroxide to form ionic bonds. As the zeta potential remains the same in all the experiments, there is no chemical interaction between the aluminium hydroxide precipitate and the pollutants. Nevertheless, the pollutants may be removed by the van der Waals interaction and hydrogen bonding. This kind of attraction does not need any change of zeta potential.<sup>28</sup> As the results showed in Section 3.2.1, zeta potential values changed with time, indicating that the chemical interaction happened. The characterization of the sludge which formed after electrocoagulation sheds light on the type of reaction happening throughout the EC process. The composition of the sludge was analyzed using the XRD spectrum two times, first for the static case (0 rpm) and second for the rotation case (150 rpm), keeping the other conditions constant ( $CD = 4 \text{ mA cm}^{-2}$ ,  $RT = 10 \text{ min}$ ,  $pH = 7$ ). As a result shown in Fig. 6a for the static case, the aluminium coagulant showed a very broad spectrum and no peaks. This broad spectrum indicates that the coagulant is amorphous or at best very poorly crystalline in nature.<sup>31</sup> It is reported that the crystallization of aluminium hydroxide is a slow process resulting in all aluminium hydroxides being either amorphous or very poorly crystalline.<sup>32</sup> As seen in Fig. 6b for the optimum rotational case (150 rpm), the crystallization took place, and the strong peaks appeared at 13, 27, 28, 38, 49 and 65 degrees, which were identified as new products, namely aluminum isobutyrate and aluminum trimethylate. Other peaks that appeared at 18.75, 20.25, 53 and 57.25 degrees were identified as aluminum oxide carbide. According to these element products, the adsorption between the colour and  $\text{Al}(\text{OH})_3$  was chemo-adsorption. Moreover, it was clear that an oxidation reaction first took place between the colour and  $\text{Al}(\text{OH})_3$ , leading to breakage of the aromatics rings of the colour to produce an aliphatic substrate as shown in Fig. 6c and the XRD result. Hence, it is clear that the reaction of the coagulant generated no aromatic products such as benzene, phenol, benzoquinone, *etc.* It is well known that aliphatic chemicals are more environmentally friendly than aromatic sludge.

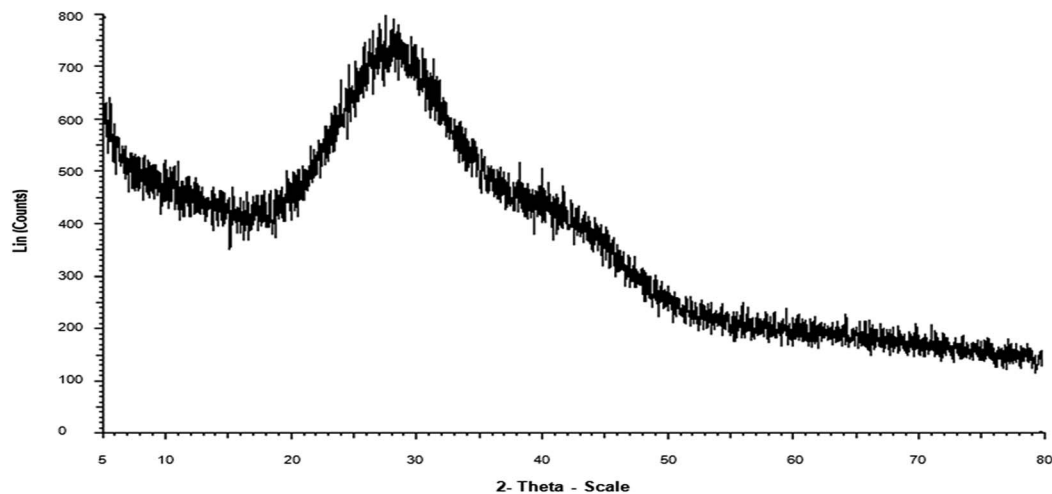
### 3.3. Hydrogen gas production

In this study, EC was used for generating hydrogen gas, contributing an advantageous revenue, as a result of electrolytic dissociation of water by connecting the EC closed reactor with an  $\text{H}_2$  detector. At the optimal current density ( $4 \text{ mA cm}^{-2}$ ), the effect of the rotational speed of the anode (0, 75, 100, 150, 200, 250 rpm) on  $\text{H}_2$  production was investigated along with the reaction time of the treatment. The  $\text{H}_2$  detector determined the amount of hydrogen as the product of the gas volume in

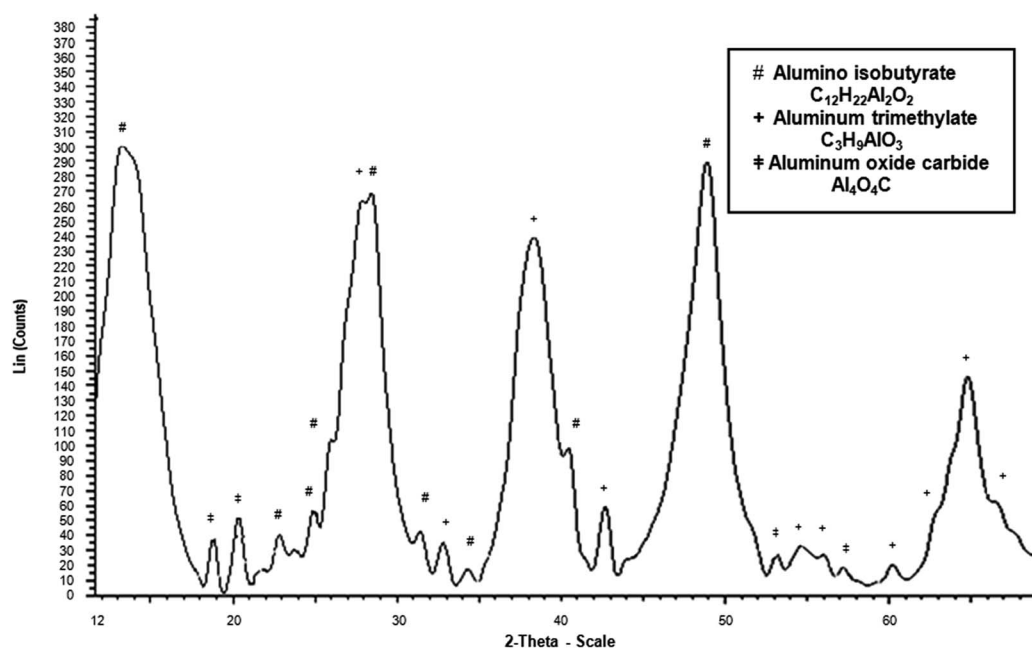
percent. At the start-up, the gas was a mixture of hydrogen and air inside the reactor. The purity of the hydrogen improves with the operating time because the generated hydrogen replaces the air in the system. As seen in Fig. 7, the volume percentage of hydrogen production during the EC process increased significantly from 9.25% to 12.45% at the first 10 min and from 26% to 35% at the 30 min reaction time when the rotational speed of the anode increased from 0 to 150 rpm respectively. The maximum values of  $\text{H}_2$  production were found at 150 rpm along the reaction time of the EC process. However, when the rotational speed was increased to 200 and 250 rpm, no increase of  $\text{H}_2$  production was observed, probably due to the extremely high rotational speed, although the quantities of  $\text{H}_2$  production were still higher than the values produced in the static case. Table 2 shows the amount of theoretical hydrogen and the amounts of hydrogen harvested from the EC process with respect to rotational speeds under the same optimal conditions ( $CD = 4 \text{ mA cm}^{-2}$ ,  $RT = 10 \text{ min}$ ). The yield of hydrogen is described as the ratio between the theoretical amount of hydrogen and the amount of hydrogen obtained from the experiment. The experimental values of  $\text{H}_2$  ( $n_{\text{H}_2}$  in mol) were calculated from eqn (11) as a result, of the values measured by the  $\text{H}_2$  detector ( $V_{\text{H}_2}$  in L) while the theoretical value was calculated from eqn (9) as the quantity ( $n_{\text{H}_2}$  in mol) and then from eqn (11) as the volume ( $V_{\text{H}_2}$  in L).

For the static case of the anode (0 rpm), the hydrogen yield was 0.73. That is, exactly 23% of the theoretical amount of hydrogen was lost in the solution. The hydrogen yield was enhanced for the rotational case to nearly 1 at 150 rpm. It is obvious that there was a large difference between the theoretical and experimental amount of  $\text{H}_2$ , but there was no significant difference in the rotation case. This is attributed to the reaction rates and current efficiencies in the rotational case being higher than the static case because the passivity phenomenon was less in the rotational case.<sup>12,14</sup> Based on the energy yield of hydrogen of  $122 \text{ kJ g}^{-1}$  and  $1 \text{ kW h} = 3600 \text{ kJ}$ , the energy content of the collected hydrogen was calculated by eqn (12).<sup>24</sup> As a result, for the amounts of  $\text{H}_2$  ( $m_{\text{H}_2}$  in g) with respect to the rotational speed of the anode, the maximum energy content ( $E_{\text{H}_2}$ ) was  $0.047 \text{ kW h m}^{-3}$  at 150 rpm, which can reduce the electrical energy consumption of the EC process by 9.4%. The electrical energy consumption of the EC process depends on the electrochemical system resistance.

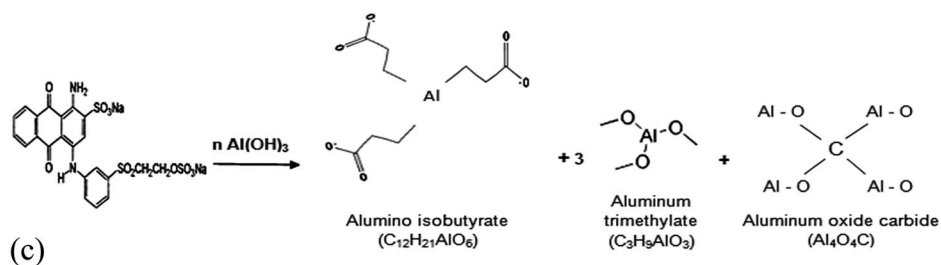
Previous studies have reported the production of  $\text{H}_2$  using the EC process for the same reaction time as in this study (10 min). Phalakornkule *et al.* (2010) reported that the energy yield of the collected hydrogen could reduce the electrical energy demand of the EC process by 8.5% when using iron electrodes with a large surface area of  $5625 \text{ cm}^2$ , and high current (16 A) for treating a low working volume (4.42 L) of reactive blue 140.<sup>10</sup> Mollah *et al.* (2004) investigated  $\text{H}_2$  production to produce an energy content of  $0.221 \text{ kW h m}^{-3}$  using iron electrodes with a surface area of  $502 \text{ cm}^2$  and a high current (8 A) for treating a solution of Orange II azo-dye.<sup>33</sup> In our study, the applied current is considered low (2 A), and the surface area of the electrodes was  $500 \text{ cm}^2$  for treating a large working volume (10 L) of real textile wastewater. As discussed in Section 3.1.1, under



(a)



(b)



(c)

Fig. 6 XRD analysis of sludge product after EC process at conditions ( $4 \text{ mA cm}^{-2}$ ,  $\text{RT} = 10 \text{ min}$ ): (a) 0 rpm; (b) 150 rpm; (c) the suggested equation of EC reaction at optimal conditions according to the XRD products.

the same current density, the rotational speed factor caused enhanced electrolytic dissociation of water, leading to increased hydrogen production and metal hydroxides to be utilized for the

removal of pollutants in the electrolytes by creating turbulence that reduced the accumulation of  $\text{H}_2$  and  $\text{O}_2$  bubbles on the surface of the electrode.

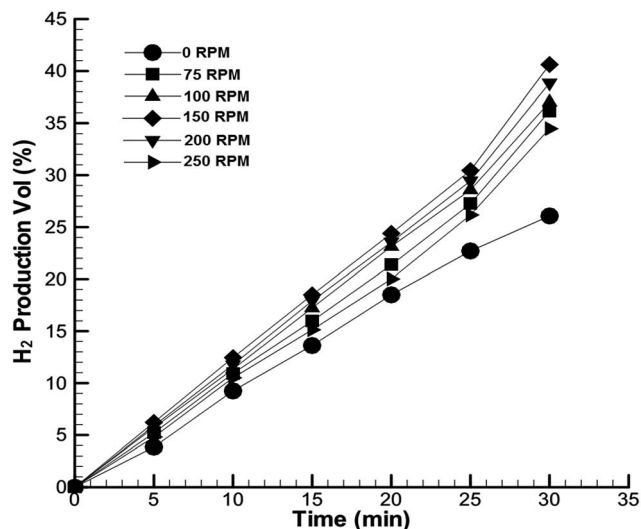
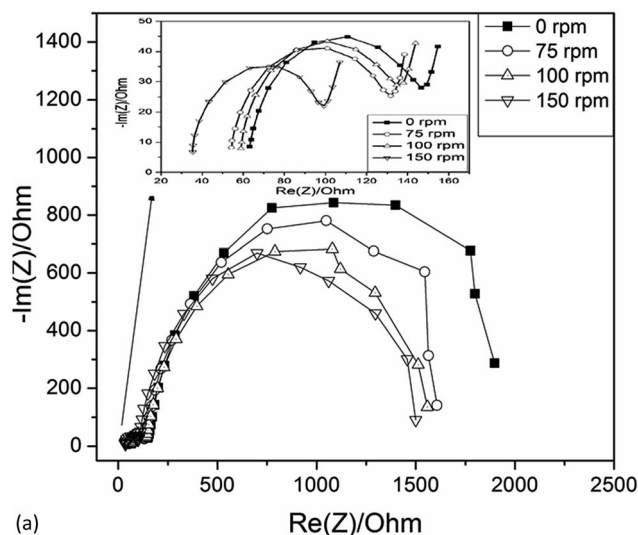


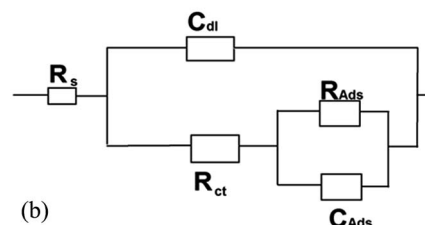
Fig. 7 Effect of anode rotational speed on  $H_2$  production as a volume percent of gas with respect to reaction time at conditions ( $CD = 4 \text{ mA cm}^{-2}$ ,  $\text{pH}$  of wastewater = 7).

### 3.4. Passivation and adsorption phenomenon

Electrochemical impedance spectroscopy is one of the most efficient techniques used to investigate the electrochemical parameters of the electrode/electrolyte interface.<sup>34,35</sup> The impedance technique was used to investigate the effect of the electrode's rotational speed (rpm) on electrode passivity and colour adsorption on the aluminium anode. The electrolyte was real textile wastewater and the potential of 0 V vs. Ag/AgCl, as well as a frequency range of 0.01– $10^5$  Hz were used to evaluate the performance of the anode/electrolyte interface. Fig. 8a shows the Nyquist plot for the anode at different rotational speeds (0, 75, 100, and 150 rpm). Two semicircles were observed at high frequencies and low frequencies. The best fits for the aluminium electrode impedance spectra are shown in Fig. 8b. The fitting parameters consisted of the solution resistance ( $R_s$ ), which was in parallel with a combination of the impedance of the faradic reaction and double layer capacitance ( $C_{dl}$ ). Other than that, the faradic reaction impedance consisted of passivation resistance ( $R_{ct}$ ), together with adsorption resistance ( $R_{ads}$ ) and adsorption capacitance ( $C_{ads}$ ).<sup>36–38</sup> Table 3 summarizes the



(a)



(b)

Fig. 8 (a) Nyquist plots of the aluminium anode in an aqueous solution of textile wastewater at different electrode rotation speed and 25 °C temperature; (b) equivalent circuits used in the fitting of the Nyquist plots.

impedance parameters. Meanwhile, the diameter of the first semicircle represents the values of  $R_{ct}$  and the second semicircle diameter represents the values of  $R_{ads}$ .

It is obvious from Fig. 8a and Table 3 that the values of  $R_{ct}$  and  $R_{ads}$  decreased significantly with the increase in the rotation speed of the aluminium anode from 0 reaching a minimum at 150 rpm. This revealed that the anode-fouling rate becomes less, and the colour adsorption rate to the anode interface becomes higher at 150 rpm. On the other hand, the maximum values of the double layer capacitance and adsorption capacitance occurred at 150 rpm. So, this explains the high removal rate when the anode is rotated at 150 rpm during the EC process

Table 2 Values of experimental, theoretical hydrogen yields and energy content with different rotational speed (rpm) at conditions ( $CD = 4 \text{ mA cm}^{-2}$ ,  $RT = 10 \text{ min}$ )

Theoretical amount of $H_2$		Experimental amount of $H_2$				$H_2$ yield	Energy content
$n_{H_2}$ (mol)	$V_{H_2}$ (L)	Rotational speed (rpm)	$n_{H_2}$ (mol)	$m_{H_2}$ (g)	$V_{H_2}$ (L)	(Experimental/theoretical)	$E_{H_2} \times 10^{-2}$ (kW h $m^{-3}$ )
0.0062	0.15	0	0.0045	0.009	0.110	0.73	346
		75	0.0053	0.0106	0.130	0.87	407
		100	0.0055	0.0110	0.135	0.90	422
		150	0.0061	0.0122	0.148	0.99	470
		200	0.0058	0.0116	0.140	0.93	446
		250	0.0052	0.0104	0.125	0.83	399

**Table 3** Electrochemical impedance data extracted from the Nyquist plots at different rotational speed (rpm)

Rotational speed (rpm)	$R_s$ ( $\Omega$ )	$R_{ct}$ ( $\Omega$ )	$C_{dl}$ ( $\mu\text{F}$ )	$R_{ads}$ ( $\Omega$ )	$C_{ads}$ ( $\mu\text{F}$ )
0	63.30	96.98	0.128	1774	7.18
75	56.90	88.89	0.129	1531	7.36
100	59.08	90.00	0.145	1369	7.13
150	40.54	41.65	0.412	1151	8.31

and validates that the model design can solve the problem statement of the previous model.

## 4. Conclusions

The EC process using a relatively new reactor was shown to be an efficient treatment for highly polluted textile wastewater. The overall findings of this study can be summarized as follows:

(1) Removal efficiencies of textile wastewater contaminants with relatively high values (91% COD, 95% colour) were obtained with a relatively low current density  $CD = 4 \text{ mA cm}^{-2}$ , during the initial 10 minutes of reaction time at an anode rotational speed of 150 rpm. The overall electrical energy consumption was  $0.56 \text{ kW h m}^{-3}$ , which resulted in lower operational costs of  $0.072 \text{ US\$ per m}^3$ , which can be considered low compared with previous studies.

(2) In the first EC half, the wastewater recirculation rate affected the elimination of colour and the COD, in addition to which higher removal efficiencies were found when reducing the recirculation flow rate. An experiment was carried out with wastewater continuously flowing over the reactor to determine the impact of the flow regime in optimal conditions of the EC batch reactor. COD and colour removal efficiencies of 91.5% and 95.5% were obtained respectively with just one pass of wastewater.

(3) The zeta potential values with time indicate that the chemical interaction happened and showed that the optimum reaction time was 10 min because after that time there was only a low increase in the zeta potential, which also indicates stabilization of the solution when the COD removal is slow in the stable stage.

(4) The EC process presents the dual advantages of (a) producing sludge without any environmental hazards, as the XRD analysis shows aliphatic chemicals in the sludge produced after treatment, and (b) enhancing the hydrogen production under the same current density using an anode rotational speed at a minimum operating area to working volume ratio, whereby the reduction in power consumption was 9.4%.

(5) The impedance results show a significant reduction in passivation of the anode and an increase in the adsorption when the anode is rotated. This explains the high removal rate in the case of the rotating anode, specifically at 150 rpm, during the EC process.

## Acknowledgements

The authors thank Master Wan Batik Sdn Bhd, a textile producer in Kajang, Kuala Lumpur, Malaysia for supplying the

textile wastewater. They also thank Universiti Teknologi Malaysia and Ministry of Education Malaysia for funding this research under Research University Grant, Vote number: Q.K130000.2510.10H26.

## References

- 1 F. Janpoor, A. Torabian and V. Khatibikamal, *J. Chem. Technol. Biotechnol.*, 2011, **86**, 1113–1120.
- 2 S. K. Verma, V. Khandegar and A. K. Saroha, *J. Hazard., Toxic Radioact. Waste*, 2013, **17**(2), 146–152.
- 3 N. Adhoum, L. Monser, N. Bellakhal and J.-E. Belgaied, *J. Hazard. Mater.*, 2004, **112**, 207–213.
- 4 U. T. Un, A. S. Kopalal and U. B. Ogutveren, *J. Environ. Manage.*, 2009, **90**, 428–433.
- 5 X. Chen, G. Chen and P. L. Yue, *Sep. Purif. Technol.*, 2000, **19**, 65–76.
- 6 B. Al Aji, Y. Yavuz and A. S. Kopalal, *Sep. Purif. Technol.*, 2012, **86**, 248–254.
- 7 I. Kabdaşlı, T. Arslan, T. Ölmez-Hancı, I. Arslan-Alaton and O. Tünay, *J. Hazard. Mater.*, 2009, **165**, 838–845.
- 8 S. Bayar, Y. Ş. Yıldız, A. E. Yılmaz and Ş. İrdemez, *Desalination*, 2011, **280**, 103–107.
- 9 M. Kobya, E. Senturk and M. Bayramoglu, *J. Hazard. Mater.*, 2006, **133**, 172–176.
- 10 C. Phalakornkule, P. Sukkasem and C. Mutchimsattha, *Int. J. Hydrogen Energy*, 2010, **35**, 10934–10943.
- 11 A. Dalvand, M. Gholami, A. Joneidi and N. M. Mahmoodi, *Clean: Soil, Air, Water*, 2011, **39**, 665–672.
- 12 V. Khandegar and A. K. Saroha, *J. Environ. Manage.*, 2013, **128**, 949–963.
- 13 A. S. Naje, S. Chelliapan, Z. Zakaria and S. A. Abbas, *Int. J. Electrochem. Sci.*, 2015, **10**, 5924–5941.
- 14 M. Y. Mollah, P. Morkovsky, J. A. Gomes, M. Kesmez, J. Parga and D. L. Cocke, *J. Hazard. Mater.*, 2004, **114**, 199–210.
- 15 B. Merzouk, M. Yakoubi, I. Zongo, J.-P. Leclerc, G. Paternotte, S. Pontvianne and F. Lapique, *Desalination*, 2011, **275**, 181–186.
- 16 M. Chafi, B. Gourich, A. Essadki, C. Vial and A. Fabregat, *Desalination*, 2011, **281**, 285–292.
- 17 U. T. Un and E. Aytac, *J. Environ. Manage.*, 2013, **123**, 113–119.
- 18 E. El-Ashtoukhy, Y. El-Taweel, O. Abdelwahab and E. Nassef, *Int. J. Electrochem. Sci.*, 2013, **8**, 1534–1550.
- 19 U. T. Un, A. S. Kopalal and U. B. Ogutveren, *Chem. Eng. J.*, 2013, **223**, 110–115.
- 20 C. Gutiérrez-Torres and J. Jiménez-Bernal, *Int. J. Electrochem. Sci.*, 2013, **8**, 274–289.
- 21 M. Rahimi, S. Amraei and A. A. Alsairafi, *Korean J. Chem. Eng.*, 2011, **28**, 1372–1379.
- 22 APHA, *Standard methods for the examination of water and wastewater*, 1998, vol. 20.
- 23 S. A. Abdel-Gawad, A. M. Baraka, K. A. Omran and M. M. Mokhtar, *Int. J. Electrochem. Sci.*, 2012, **7**, 6654–6665.
- 24 F. Kargi, E. C. Catalkaya and S. Uzuncar, *Int. J. Hydrogen Energy*, 2011, **36**, 2049–2056.
- 25 S. Aoudj, A. Khelifa, N. Drouiche, M. Hecini and H. Hamitouche, *Chem. Eng. Process.*, 2010, **49**, 1176–1182.

- 26 M. A. Ajeel, M. K. Aroua and W. M. A. W. Daud, *Electrochim. Acta*, 2015, **169**, 46–51.
- 27 M. M. Emamjomeh and M. Sivakumar, *J. Environ. Manage.*, 2009, **90**, 1204–1212.
- 28 Z. Zaroual, M. Azzi, N. Saib and E. Chaïnet, *J. Hazard. Mater.*, 2006, **131**, 73–78.
- 29 P. K. Holt, G. W. Barton, M. Wark and C. A. Mitchell, *Colloids Surf., A*, 2002, **211**, 233–248.
- 30 M. M. Emamjomeh, *Electrocoagulation technology as a process for defluoridation in water treatment*, 2006.
- 31 S. Vasudevan, B. S. Kannan, J. Lakshmi, S. Mohanraj and G. Sozhan, *J. Chem. Technol. Biotechnol.*, 2011, **86**, 428–436.
- 32 D. Ghosh, C. Medhi and M. Purkait, *Chemosphere*, 2008, **73**, 1393–1400.
- 33 M. Y. Mollah, S. R. Pathak, P. K. Patil, M. Vayuvegula, T. S. Agrawal, J. A. Gomes, M. Kesmez and D. L. Cocke, *J. Hazard. Mater.*, 2004, **109**, 165–171.
- 34 C. M. Brett and A. O. Brett, *Principles, Electrochemistry, Methods and Applications*, Oxford University Press, Oxford, 1993.
- 35 S. C. B. Oliveira and A. M. Oliveira-Brett, *Electrochim. Acta*, 2010, **55**, 4599–4605.
- 36 A. Sakharova, L. Nyikost and Y. Pleskov, *Electrochim. Acta*, 1992, **37**, 973–978.
- 37 J. Hernando, S. Q. Lud, P. Bruno, D. M. Gruen, M. Stutzmann and J. A. Garrido, *Electrochim. Acta*, 2009, **54**, 1909–1915.
- 38 Z. Bo, Z. Wen, H. Kim, G. Lu, K. Yu and J. Chen, *Carbon*, 2012, **50**, 4379–4387.